Article

Intermolecular Electron-Transfer Mechanisms via Quantitative Structures and Ion-Pair Equilibria for Self-Exchange of Anionic (Dinitrobenzenide) Donors

Sergiy V. Rosokha, Jian-Ming L, Marshall D. Newton, and Jay K. Kochi

J. Am. Chem. Soc., **2005**, 127 (20), 7411-7420• DOI: 10.1021/ja051063q • Publication Date (Web): 30 April 2005

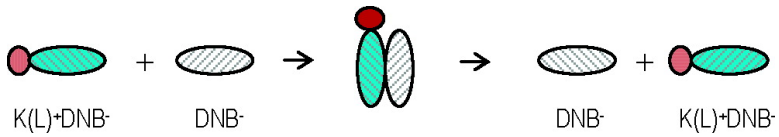

More About This Article

Additional resources and features associated with this article are available within the HTML version:

- Supporting Information
- Links to the 10 articles that cite this article, as of the time of this article download
- Access to high resolution figures
- Links to articles and content related to this article
- Copyright permission to reproduce figures and/or text from this article

View the Full Text HTML

J|A|C|S
ARTICLES
Published on Web 04/30/2005

Intermolecular Electron-Transfer Mechanisms via Quantitative Structures and Ion-Pair Equilibria for Self-Exchange of Anionic (Dinitrobenzenide) Donors

Sergiy V. Rosokha, Jian-Ming Lü, Marshall D. Newton, and Jay K. Kochi*

Contribution from the Department of Chemistry, University of Houston, Houston, Texas, 77204, and Department of Chemistry, Brookhaven National Laboratory, Upton, New York, 11973

Received February 18, 2005; E-mail: jkochi@uh.edu

Abstract: Definitive X-ray structures of "separated" versus "contact" ion pairs, together with their spectral (UV−NIR, ESR) characterizations, provide the quantitative basis for evaluating the complex equilibria and intrinsic (self-exchange) electron-transfer rates for the potassium salts of *p*-dinitrobenzene radical anion (DNB^-). Three principal types of ion pairs, $K(\mathbf{L})^+DNB^-$, are designated as Classes S, M, and C via the specific ligation of K^+ with different macrocyclic polyether ligands (**L**). For Class S, the self-exchange rate constant for the separated ion pair (SIP) is essentially the same as that of the "free" anion, and we conclude that dinitrobenzenide reactivity is unaffected when the interionic distance in the separated ion pair is $r_{SIP} \geq 6$ Å. For Class M, the dynamic equilibrium between the contact ion pair (with $r_{CIP} = 2.7$ Å) and its separated ion pair is quantitatively evaluated, and the rather minor fraction of SIP is nonetheless the principal contributor to the overall electron-transfer kinetics. For Class C, the SIP rate is limited by the slow rate of CIP ⇄ SIP interconversion, and the self-exchange proceeds via the contact ion pair by default. Theoretically, the electron-transfer rate constant for the separated ion pair is well-accommodated by the Marcus/Sutin two-state formulation when the precursor in Scheme 2 is identified as the "separated" inner-sphere complex (IS_{SIP}) of cofacial DNB^-/DNB dyads. By contrast, the significantly slower rate of self-exchange via the contact ion pair requires an associative mechanism (Scheme 3) in which the electron-transfer rate is strongly governed by cationic mobility of $K(\mathbf{L})^+$ within the "contact" precursor complex (IS_{CIP}) according to the kinetics in Scheme 4.

Introduction

Anionic reagents are among the most effective electron donors (reductants) in both inorganic as well as organic redox systems; likewise, the best electron acceptors (oxidants) are commonly found to be cationic species.[1,2] As a result, it has long been recognized that the ion-pairing effects can play critical roles in mediating electron-transfer rates of charged donors and acceptors in solutions.[3] However, such studies have been necessarily limited to qualitative descriptions of dynamic ion pairs owing to equilibration among various ionic structures that is readily subject to solvent effects.[4,5]

Among various spectroscopic techniques, ESR offers a versatile and useful probe for the dynamic behavior of various ions since quantitative changes in odd-electron (spin) distribution, especially of paramagnetic organic species, can be directly evaluated in solution. Thus, Weissman, Hirota, Szwarc, and coworkers[6−8] were among the first to examine intermolecular electron transfer from different organic anion radicals and to establish the presence of at least two principal types of ion pairs from their distinctive ESR spectra. In particular, Hirota found aromatic anion radicals to exist as "free" anions or "loose" ion pairs (with alkali metal cations) that show high electron-transfer rates, as well as "tight" ion pairs that show significantly

(1) (a) Astruc, D. In *Electron Transfer in Chemistry*; Balzani, V., Ed.; Wiley-VCH: New York, 2001; Vol. 2, p 714. (b) Donohoe, T. J. *Oxidation and Reduction in Organic Synthesis*; Oxford University Press: New York, 2000. (c) Kenneth, L. R., Jr. *Oxidation and Reduction of Organic Compounds*; Prentice-Hall: Englewood Cliffs, NJ, 1973. (d) Rathore, R.; Kochi, J. K. *Adv. Phys. Org. Chem.* **2000**, *35*, 193.

(2) (a) Eberson, L. *Electron-Transfer Reactions in Organic Chemistry*; Springer-Verlag: New York, 1987. (b) Connelly, N. G.; Geiger, W. E. *Adv. Organomet. Chem.* **1984**, *23*, 1.

(3) (a) *Ions and Ion Pairs in Organic Reactions*; Szwarc, M., Ed.; Wiley-Interscience: New York, 1972; Vols. 1 and 2. (b) Gordon, J. E. *Organic Chemistry of Electrolyte Solutions*; Wiley: New York, 1975. (c) Loupy, A.; Tchoubar, B. *Effets des Sales en Chimie Organique et Organometallique*; Dunod University: Paris, 1988. (d) Kosower, E. M. *Introduction to Physical Organic Chemistry*; Wiley: New York, 1968. (e) Kaiser, E. T.; Kevan, L. *Radical Ions*; Interscience: New York, 1968. (f) Peters, S. J.; Turk, M. R.; Kiesewetter, M. K.; Reiter, R. C.; Stevenson, C. D. *J. Am. Chem. Soc.* **2003**, *125*, 11212. (g) Batz, M. L.; Garland, P. M.; Reiter, R. C.; Sandborn, M. D.; Stevenson, C. D. *J. Org. Chem.* **1997**, *62*, 2045.

(4) (a) Marcus, R. A. *J. Phys. Chem. B* **1998**, *102*, 10071. (b) Chen, P.; Meyer, T. J. *Chem. Rev.* **1998**, *98*, 1439. (c) Piotrowiak, P.; Miller, J. R. *J. Phys. Chem.* **1993**, *97*, 13052. (d) Vakarin, E. V.; Holovko, M. F.; Piotrowiak, P. *Chem. Phys. Lett.* **2002**, *363*, 7.

(5) (a) Sorensen, S. P.; Bruning, W. H. *J. Am. Chem. Soc.* **1973**, *95*, 2445. (b) Brown, G. M.; Sutin, N. *J. Am. Chem. Soc.* **1979**, *101*, 884. (c) Piotrowiak, P. *Inorg. Chim. Acta* **1994**, *225*, 269. (d) Pfeiffer, J.; Kirchner, K.; Wherland, S. *Inorg. Chim. Acta* **2001**, *313*, 37. (e) Nelsen, S. F.; Ismagilov, R. F. *J. Phys. Chem. A* **1999**, *103*, 5373. (f) Telo, J. P.; Grampp, G.; Shohoji, M. C. B. L. *Phys. Chem. Chem. Phys.* **1999**, *1*, 99. (g) Okamoto, K.; Imahori, H.; Fukuzumi, S. *J. Am. Chem. Soc.* **2003**, *125*, 7014. (h) Grigoriev, V. A.; Cheng, D.; Hill, C. L.; Weinstock, I. A. *J. Am. Chem. Soc.* **2001**, *123*, 5292. (i) Saveant, J.-M. *J. Phys. Chem. B* **2001**, *105*, 8995. (j) Andrieux, C. P.; Robert, M.; Saveant, J.-M. *J. Am. Chem. Soc.* **1995**, *117*, 9340.

(6) Zandstra, P. J.; Weissman, S. I. *J. Am. Chem. Soc.* **1962**, *84*, 4408.

(7) (a) Hirota, N.; Carraway, R.; Schook, W. *J. Am. Chem. Soc.* **1968**, *90*, 3611. (b) Hirota, N. *J. Am. Chem. Soc.* **1968**, *90*, 3603. (c) Hirota, N. *J. Phys. Chem. Soc.* **1967**, *71*, 127.

(8) Karasawa, Y.; Levin, G.; Szwarc, M. *J. Am. Chem. Soc.* **1971**, *93*, 4614.

diminished reactivity. Interestingly, Hirota also assigned the negative temperature dependence of the electron-transfer kinetics to the fast equilibration between tight and loose ion pairs. Otherwise, no clear mechanistic delineation of ion-pairing effects on electron transfer has been forthcoming. Although ESR measurements do provide some guide as to the interionic separations extant in tight and loose ion pairs, sensitivity in most cases is insufficient to afford quantitative information of value for mechanistic studies.

We recently showed how the two principal types of interionic assemblies, hereinafter referred to as "separated" (loose) and "contact" (tight) ion pairs, can be isolated as pure crystalline salts suitable for direct X-ray analysis.[9] The successful isolation and X-ray structures of the separated ion pair (SIP) and contact ion pair (CIP) now allow us to quantitatively evaluate the electron-transfer efficiency of donor anions without structural ambiguities of their ion pairs inherent to all previous studies.[4−8] As such, we will focus on how the use of various ligands (**L**) including [2,2,2]cryptand and three 18-crown-6-ethers affects (1) the different reactivities of the separated and contact ion pairs of *p*-dinitrobenzenide anions (DNB^-) and (2) the overall (phenomenological) electron-transfer rates as modulated by the reversible interchange between SIP and CIP assemblies in solution.

I. Quantitative Effects of Polyether Ligands on Ion-Pair Structures and Equilibria. The macrocyclic polyether ligands (**L**) can be classified into three categories according to their effectiveness in encapsulating and isolating the potassium cation: Class S where the ligand is [2,2,2] cryptand to form the separated ion pair, K(**cryptand**)$^+$//DNB^-; Class C where the ligand is dibenzo-18-crown-6 (or simply **BC**) to form the strong contact ion pair, K(**BC**)$^+DNB^-$; and Class M where the ligand is either 18-crown-6 (**C**) or di-cyclohexano-18-crown-6 (**HC**) to form the moderated contact ion pairs, K(**C**)$^+DNB^-$ or K(**HC**)$^+DNB^-$, in mobile equilibrium with the separated ion pairs, K(**C**)$^+$//DNB^- or K(**HC**)$^+$//DNB^- as follows.

Class S. The separated ion pair of dinitrobenzenide can be prepared by the potassium-mirror reduction of *p*-dinitrobenzene in the presence of the three-dimensional cryptand, and the complexed [1:1] salt is isolated as K(**cryptand**)$^+$//DNB^- with the wide interionic separation of $r_{SIP} \geq 6$ Å.[10] The anionic moiety in this separated ion pair has a distinctive near-IR absorption ($\lambda_{IV} = 915$ nm) with a characteristic vibronic fine structure in THF solution (Figure S1, Supporting Information). This spectrum is singularly invariant with temperature changes between +30 and −90 °C, and it is essentially the same as the NIR spectrum of "free" dinitrobenzenide anion prepared in the more polar DMF solvent.[11] Moreover, such a loosely bound ion-pair structure persists in THF solution, as indicated by the unchanged vibronic fine structure measured in the crystalline solid state relative to that of crystals dissolved into THF.[10]

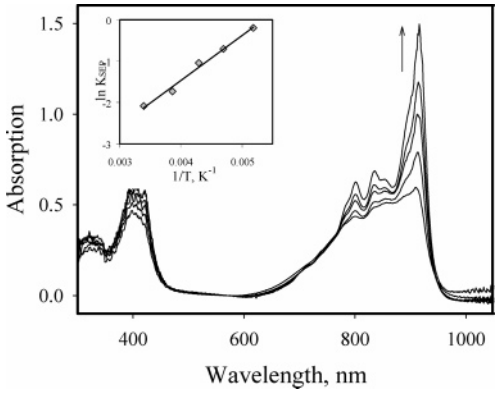

Figure 1. Temperature-dependent UV−NIR spectrum of K(**C**)$^+DNB^-$ in THF measured at (bottom to top) 295, 259, 233, 213, and 190 K. Inset: Inverse temperature dependence of the ion-pair separation.

Class C. The "contact" ion pair of dinitrobenzenide can be prepared by an analogous reduction, but in the presence of the *two*-dimensional crown ether **BC** and the [1:1] salt isolated as K(**BC**)$^+DNB^-$ with the close interionic separation of $r_{CIP} = 2.7$ Å.[10,12] The contact ion pair K(**BC**)$^+DNB^-$ shows a different vibronic fine structure that is also temperature-invariant and unchanged upon dissolution of the crystals into THF (Figure S1), as expected for the tightly bound contact ion pair not readily prone to ionic separation in solution.

Class M. In the intermediate region, crown-ether ligands **C** and **HC** lead to contact ion pairs K(**C**)$^+DNB^-$ and K(**HC**)$^+$-DNB^-, which are subject to marked spectral changes with temperature between +20 and −90 °C; the NIR spectrum at the higher temperature of +20 °C is rather close to that of contact ion pair K(**BC**)$^+DNB^-$ in Class C, whereas at the low-temperature limit of −90 °C the NIR spectrum resembles that of the separated ion pair K(**cryptand**)$^+$//DNB^- in Class S. Each ion-pair structure shows characteristic near-IR bands arising from the intervalence transition in the dinitrobenzenide moiety,[10] and thus the equilibration among Class S, C, and M ion pairs is readily measured by temperature-dependent spectral changes (Figure 1). Quantitative evaluation of these spectral changes (see inset, Figure 1) indicates the facile (reversible) equilibrium that increasingly favors ion-pair separation at decreasing temperatures,[13] that is:

$$\underset{\text{(CIP)}}{K(\mathbf{C})^+DNB^-} \overset{K_{SEP}}{\rightleftharpoons} \underset{\text{(SIP)}}{K(\mathbf{C})^+//DNB^-} \qquad (1)$$

(9) (a) Davlieva, M. G.; Lü, J. M.; Lindeman, S. V.; Kochi, J. K. *J. Am. Chem. Soc.* **2004**, *126*, 4557. (b) For *operational* distinction between "separated" and "contact" ion pairs, see footnote 17 in ref 10. (c) The thermodynamic (and kinetics) justification for two principal types of such dynamic ion pairs is presented by Szwarc[3a] (Vol. 1, p 1 ff).

(10) Lü, J.-M.; Rosokha, S. V.; Lindeman, S. V.; Neretin, I. S.; Kochi, J. K. *J. Am. Chem. Soc.* **2005**, *127*, 1797. The X-ray structure below illustrates how the interionic separation in the separated ion pair is enforced via *complete* encapsulation of potassium so that the cation is effectively insulated from the dinitrobenzenide counteranion by the wide interionic separation of ≥6 Å.

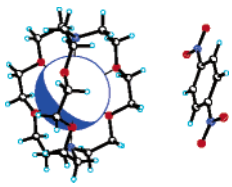

(11) Nelsen, S. F.; Konradsson, A. E.; Weaver, M. N.; Telo, J. P. *J. Am. Chem. Soc.* **2003**, *125*, 12493.

(12) The X-ray structure below illustrates how complexation of K^+ with the two-dimensional 18-crown-6 is sufficient to protect only the back face of the cationic sphere, which is then free to form the contact ion pair with dinitrobenzenide from the unprotected front face by the close interionic separation of 2.7 Å.[10]

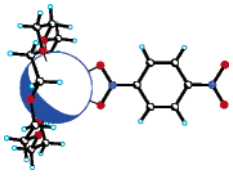

Table 1. Thermodynamics of CIP/SIP Equilibria of K(**L**)$^+$DNB$^-$ in THF Solutions[a]

L	$-\Delta H_{SEP}$ (kcal mol^{-1})	$-\Delta S_{SEP}$ (eu)	α^e
cryptand	*b*	*b*	100
C	2.2	12	0.14
HC	2.2 (1.8[c])	11 (10[c])	0.16
BC	1.4[c,d]	13[c,d]	0.015

[a] At 20 °C, based on UV−vis measurements, unless noted otherwise. [b] Only SIP observed by UV−vis and ESR spectroscopy. [c] ESR measurements. [d] Only CIP observed by UV−vis spectroscopy at 20 °C. [e] Fraction of SIP in typical 1 mM solutions of K(**L**)$^+$ DNB$^-$ in THF at 20 °C.

Digital deconvolution of the complex absorption changes by spectral superposition (see Experimental and Computational Methodologies section) allows the thermodynamic parameters for ion-pair separation to be determined as listed in Table 1, and essentially the same results are obtained with the related contact ion pair K(**HC**)$^+$DNB$^-$.[13]

II. Electronic (ESR) Structures and Dynamic Equilibria between Separated and Contact Ion Pairs. The N^{14}-hyperfine splitting in the ESR spectrum of the dinitrobenzenide anion provides a highly sensitive probe for ion-pair structures, particularly with regard to ion-pair dynamics in solution.

Class S. Upon dissolution into THF, the separated ion pair K(**cryptand**)$^+$//DNB$^-$ leads to the well-resolved ESR spectrum with $a_{2N} = 1.23$ G and $a_{4H} = 1.11$ G owing to the symmetric ground state with (static) delocalization of the unpaired electron equally over both NO_2 centers. This ESR spectrum is temperature-invariant between +20 and −90 °C, corresponding to the rather isotropic distribution of charge in the loosely bound anion.[10]

Class C. Dissolution of the contact ion-pair salt K(**BC**)$^+$-DNB$^-$ under the same conditions also leads to a well-resolved ESR spectrum but one consisting of two principal species, hereinafter designated as CIP_1 with $a_{1N} = 4.5$ G/$a_{2H} = 2.3$ G and CIP_2 with $a_{1N} = 5.0$ G/$a_{2H} = 2.5$ G. Deconvolution of the composite spectra taken at various temperatures leads to the isomerization constant of $K_{ISOM} = 5$ at 20 °C,

$$CIP_1 \overset{K_{ISOM}}{\rightleftharpoons} CIP_2 \qquad (2)$$

and the thermodynamic parameters: $\Delta H_{ISOM} = -1.5$ kcal mol^{-1} and $\Delta S_{ISOM} = -2$ eu in the temperature range −50 to +40 °C (Figure S2).[10] Careful analysis of the ESR spectrum at low temperatures (0 °C and lower) reveals the additional (minor) presence of the separated ion pair K(**BC**)$^+$//DNB$^-$ shown in Figure 2.[14a]

Class M. The THF solutions of the intermediate ion pair prepared by dissolution of either K(**C**)$^+$DNB$^-$ or K(**HC**)$^+$-DNB$^-$ afford ESR spectra of a single contact ion pair CIP_3,

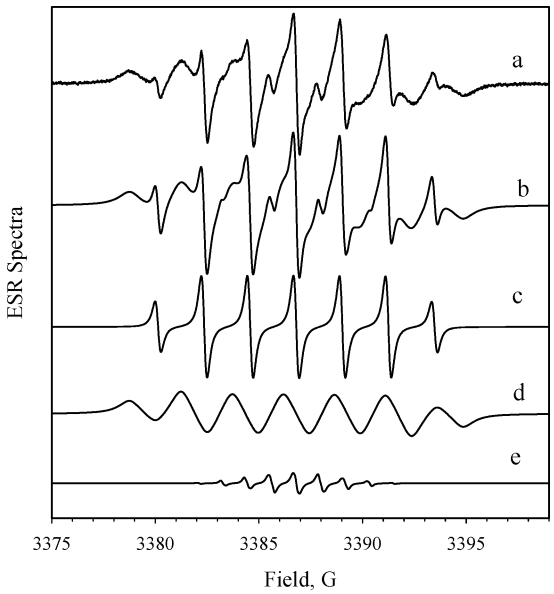

Figure 2. ESR spectrum of K(**BC**)$^+$DNB$^-$ in THF at 0 °C (a). Computer simulation (b) by the addition of three components of CIP_1(c), CIP_2 (d), and SIP (e).[14b]

both with the same value of $a_{1N} \approx 3.3$ G.[14c] Upon lowering the temperature, the solutions of K(**C**)$^+$DNB$^-$ and K(**HC**)$^+$DNB$^-$ begin to show at −50 °C the increasing growth of an additional component with ESR splitting pattern ($a_{2N} = 1.23$ G) assigned to that of the separated ion pair (SIP_3), that is:

$$CIP_3 \overset{K_{SEP}}{\rightleftharpoons} SIP_3 \qquad (3)$$

which is akin to the separated ion pair (SIP_1) from K(**cryptand**)$^+$//DNB$^-$ or equivalently (SIP_2) from K(**BC**)$^+$DNB$^-$ (low temperature).[10] Quantitative spectral deconvolution (Figure S7) leads to the separation constant in eq 1 (or eq 3) with the thermodynamic parameters $\Delta H_{SEP} = -1.7$ and -1.8 ± 0.5 kcal mol^{-1}, for the K(**C**)$^+$ and K(**HC**)$^+$ salts, respectively,[13b] and importantly, they coincide with the values independently evaluated from the UV−vis spectral data in Table 1 within the precision limits.

The contact and separated ion-pair equilibria for Class S, C, and M (dinitrobenzenide) salts are thus clearly shown by spectral evaluations to be strongly dependent on the nature and strength of the polyether ligation of the potassium cation. Since the donor properties of the separated (or free) dinitrobenzenide anion are essentially the same for all salts irrespective of the polyether ligands,[14d,e] we can now evaluate quantitatively how its electron-transfer reactivity is modulated by the ion-pair equilibria.

III. Dynamic Ion-Pair Effects on Dinitrobenzenide in Intermolecular Electron Transfer. As a mixed-valence an-

(13) (a) The equilibrium shift to SIP at low temperatures indicates that the THF solvation of K(**L**)$^+$, that is,

$$K(\mathbf{L})^+DNB^- + n\text{THF} \overset{K_D}{\rightleftharpoons} DNB^- + K(\mathbf{L})^+(\text{THF})_n \qquad (1a)$$

is accompanied by a higher enthalpy gain but disfavored by entropy relative to the ionic binding: K(**L**)$^+$DNB$^-$. A similar equilibrium shift was observed earlier in aromatic anion-radical equilibria.[7] (b) Note that $K_D = [SIP]^2/[CIP] = K_{SEP}K_{ION}$, where $K_{SEP} = [SIP]/[CIP]$ is defined by eq 1(3) and K_{ION} transforms the SIP into its free ions. Therefore, for $\alpha \ll 1$ (as observed at room temperature): $K_D = \alpha^2 c_o/(1-\alpha) \approx \alpha^2 c_o$ and $K_{SEP} = \alpha/(1-\alpha) \approx \alpha$, which leads to $\Delta H_D = R\Delta(\ln \alpha^2 c_o)/\Delta(T^{-1}) = 2R\Delta(\ln \alpha)/\Delta(T^{-1})$ and $\Delta H_{SEP} = R\Delta(\ln K_{SEP})/\Delta(T^{-1}) \approx R\Delta(\ln \alpha)/\Delta(T^{-1})$. As a result, $\Delta H_{SEP} \approx {}^1/_2\Delta H_D$, where ΔH_{SEP} (Table 1) refers to the equilibrium in eq 1(3) and ΔH_D to that in eq 1a (vide supra).

(14) (a) Relative concentrations of the separated ion pairs of dinitrobenzenide anion (determined from the ESR spectrum of K(**BC**)$^+$DNB$^-$ at various temperatures) lead to the thermodynamic parameters for CIP separation of $\Delta H_{SEP} = -1.4$ kcal mol^{-1} and $\Delta S_{SEP} = -13$ eu in Table 1. (b) Note that the line width (0.80 G) of CIP_2 is significantly larger than those of CIP_1 (0.35 G) and SIP (0.30 G) owing to the intramolecular spin exchange as described in ref 10. (c) The complex ESR spectra necessitated the use of the per-deuterio derivative of dinitrobenzene [i.e., K(**HC**)$^+$ *p*-$O_2NC_6D_4$-NO_2^-] and precluded the measurement of the proton splitting.[10] (d) As indicated, for example, by the ESR and NIR spectra of the dinitrobenzenide moiety in the separated ion pair K(**cryptand**)$^+$//DNB$^-$ in THF and of the free anion in DMF, which are the same. (e) Thus, beyond the interionic separation of $r_{DA} \geq 6$ Å, the counterion effect on dinitrobenzenide reactivity is too small to be evaluated.

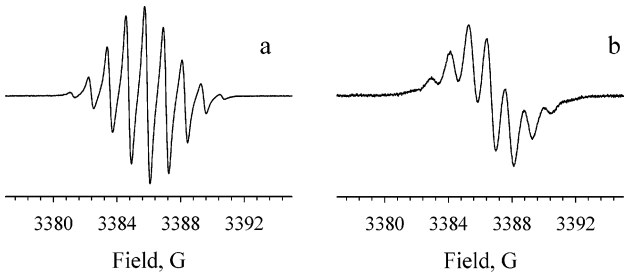

Figure 3. Typical line broadening in the ESR spectrum observed in THF solution of (a) 0.7 mM K(**cryptand**)$^+$ DNB$^{\bullet+}$ and (b) upon the addition of DNB (4 mM).

ion,[11,15] dinitrobenzenide is an effective electron donor by virtue of the reversible oxidation potential: $E_{ox}° = -0.64$ V versus SCE.[16] As such, the earliest ESR studies of dinitrobenzenide[17] revealed the diagnostic hyperfine line broadenings[18] arising from the faster rates of intermolecular (self) exchange that accompany increasing concentrations of the neutral *p*-dinitrobenzene acceptor (DNB). This convenient methodology allows the quantitative evaluation of the electron-transfer rates, and the observed (phenomenological) second-order rate constant k_2 applies to the self-exchange process:

$$DNB^{\bullet-} + DNB \xrightarrow{k_2} DNB + DNB^{\bullet-} \quad (4)$$

Class S. Stepwise addition of DNB to the THF solution of the separated ion-pair salt K(**cryptand**)$^+$//DNB$^-$ at constant temperature results in increased (general) broadening of the ESR spectrum, typically shown in Figure 3. Such a concentration-dependent line broadening of the ESR spectrum is the same as that observed earlier for the free anion (eq 4),[17,19] and it derives from the intermolecular (self-exchange) electron transfer that must directly involve only the separated ion pair (in a solvent of this low polarity), that is,

$$K(\mathbf{cryptand})^+//DNB^- + DNB \xrightarrow[THF]{k_{SIP}} DNB + K(\mathbf{cryptand})^+//DNB^- \quad (5)$$

It is to be noted that the observed second-order rate constant: $k_2 = 3.0 \times 10^9$ M^{-1} s^{-1} obtained at 20 °C (Table 2) is related to an activation barrier: $E_{SIP} = 2.5 \pm 0.5$ kcal mol^{-1} measured from the temperature dependence of k_2 in the temperature range +40 to −20 °C (Figure 4). Such a fast dynamic process approaches the limit that is characteristic of diffusion-controlled processes,[20] and if due cognizance is taken in the uncertainty in the measured values of k_2 (and E_{SIP}) for K(**cryptand**)$^+$//DNB$^-$ in THF, we are forced to conclude that the value of k_2 in eq 4 is at or very close to the diffusion-controlled limit.

Table 2. Observed Rate Constants and Activation Barriers for the Intermolecular (Electron-Transfer) Self-Exchange with Class S, C, and M Salts K(**L**)$^+$DNB$^-$ in the Presence of Added *p*-Dinitrobenzene[a]

L	k_2 (M^{-1} s^{-1})	E_a (kcal/mol)
cryptand	3.0×10^9	2.5
C	5.3×10^8	0.7
HC	4.5×10^8	−0.3
BC	6.5×10^7 [b]	5.7[b]
	1.0×10^8 [c]	6.3[c]

[a] In THF, at 20 °C. [b] For CIP$_1$. [c] For CIP$_2$.

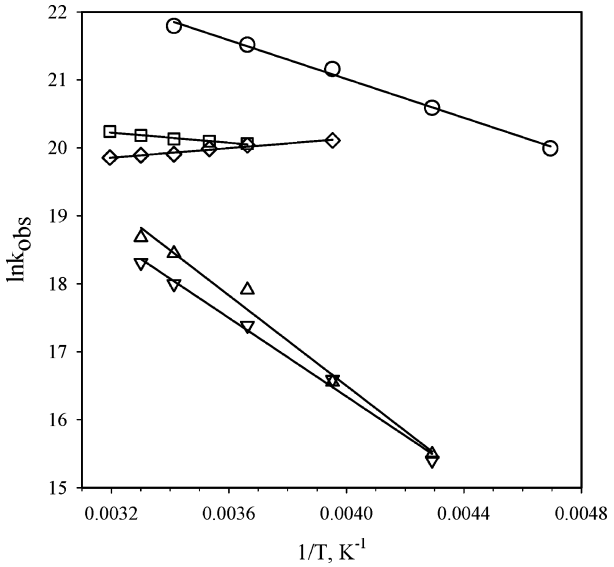

Figure 4. Arrhenius plots for DNB$^{\bullet-}$/DNB self-exchange of ion pairs containing cations K(**cryptand**)$^+$ (○), K(**C**)$^+$ (□), K(**HC**)$^+$ (◇), K(**BC**)$^+$-(CIP$_1$) (▽), and K(**BC**)$^+$ (CIP$_2$) (△) as described in the text.

Class C. In contrast to the cryptand-ligated ion pair, the line width change in the ESR spectrum of the contact ion pair derived from dibenzo-18-crown-6 K(**BC**)$^+$DNB$^-$ is rather insensitive to the addition of *p*-dinitrobenzene, and the broadening becomes apparent only at significantly higher concentrations of added acceptor (Figure 5). Digital deconvolutions of such broadened (composite) spectra at various DNB concentrations yield the substantially slower rate constants for self-exchange via the contact ion pair, that is,

$$K(\mathbf{BC})^+DNB^- + DNB \xrightarrow{k_{CIP}} DNB + K(\mathbf{BC})^+DNB^- \quad (6)$$

where $k_2 = 6.5 \times 10^7$ and 1.0×10^8 M^{-1} s^{-1} for CIP$_1$ and CIP$_2$, respectively, at 20 °C (see Experimental and Computational Methodologies section for details). Moreover, the variation of the second-order k_{CIP} in the temperature range from +30 to −30 °C leads to the activation energies $E_a = 5.7$ and 6.3 kcal mol^{-1} for CIP$_1$ and CIP$_2$, respectively, which are more than twice that evaluated for the separated ion pair K(**cryptand**)$^+$DNB$^-$.

Class M. Owing to the presence of both separated and contact ion pairs in THF solutions of the 18-crown-6 and dicyclohexano-18-crown-6 complexes K(**C**)$^+$DNB$^-$ and K(**HC**)$^+$DNB$^-$, the ESR line broadenings can be examined in the fast-exchange limits. Thus, the ESR spectra of 1 mM solutions of K(**C**)$^+$DNB$^-$

(15) For some other recent examples of organic mixed-valence systems, see: (a) Lambert, C.; Nöll, G. *J. Am. Chem. Soc.* **1999**, *121*, 8434. (b) Nelsen, S. F. *Chem.−Eur. J.* **2000**, *6*, 581. (c) Risko, C.; Barlow, S.; Coropceanu, V.; Halik, M.; Bredas, J.-L.; Marder, S. R. *Chem. Commun.* **2003**, 194. (d) Lindeman, S. V.; Rosokha; S. V.; Sun, D.-L.; Kochi, J. K. *J. Am. Chem. Soc*, **2002**, *124*, 843. (e) Rak, S. F.; Miller, L. L. *J. Am. Chem. Soc.* **1992**, *114*, 1388.

(16) In DMF, see: Chambert, J. Q.; Adams, R. N. *J. Electroanal. Chem.* **1965**, *9*, 400. In THF containing 0.1 M $Bu_4N^+PF_6^-$ as the supporting electrolyte, our CV studies showed the reversible 1-electron cathodic wave of DNB/DNB$^-$ at 0.69 V vs SCE.

(17) (a) Miller, T. A.; Adams, R. N.; Richards, P. M. *J. Chem. Phys.* **1966**, *44*, 4022. See also: (b) Layoff, T.; Miller, T. A.; Adams, R. N.; Fah, H.; Horsfield, A.; Proctor, W. *Nature* **1965**, *205*, 4969.

(18) (a) Kivelson, D. *J. Chem. Phys.* **1957**, *27*, 1087; **1960**, *33*, 1094. (b) Ward, R. L.; Weissman, S. I. *J. Am. Chem. Soc.* **1957**, *79*, 2086. (c) Zandstra, P. J.; Weissman, S. I. *J. Chem. Phys.* **1961**, *35*, 757.

(19) Hosoi, H.; Mori, Y.; Masuda, Y. *Chem. Lett.* **1998**, 178.

(20) Evaluated as $k_{diff} = 1.27 \times 10^{10}$ M^{-1} s^{-1} at 20 °C. See: Grampp, G.; Jaenicke, W. *Ber. Bunsen-Ges. Phys. Chem.* **1991**, *95*, 904.

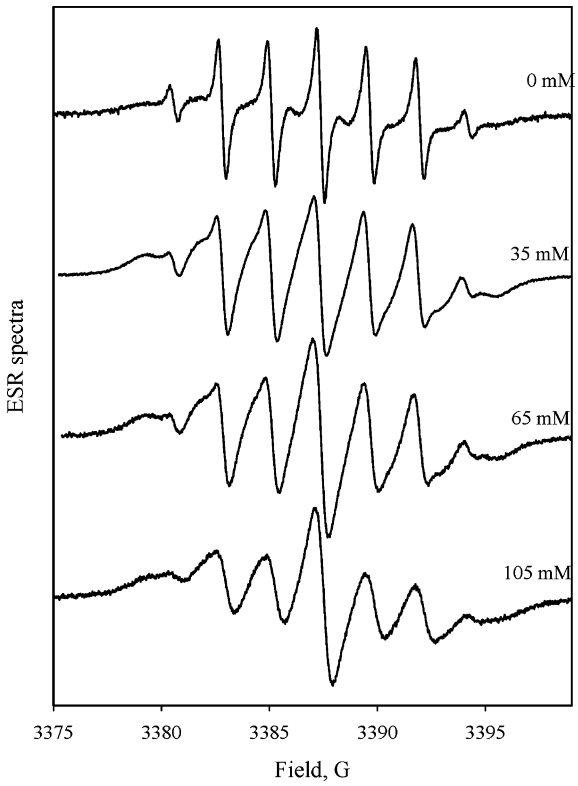

Figure 5. ESR spectral line broadening in THF solutions of K(**BC**)$^+$DNB$^-$ in the presence of neutral DNB acceptor (at concentrations indicated).

and K(**HC**)$^+$DNB$^-$ in THF showing resolved hyperfine splittings (vide supra) at 20 °C gradually broaden and then finally coalesce into a single broad envelope at the increased dinitrobenzene concentration of ~50 mM. Under these conditions, further additions of dinitrobenzene is accompanied by narrowing of the broad line, and the line widths measured at constant temperature lead to the overall second-order rate constant for intermolecular electron transfer $k_2 = 5.3 \times 10^8$ M^{-1} s^{-1} for K(**C**)$^+$DNB$^-$, and the temperature dependence of k_2 affords the limited activation energy of $E_a = +0.7$ kcal mol^{-1}. It is thus noteworthy that the overall second-order rate constant for the dicyclohexano analogue K(**HC**)$^+$DNB$^-$ of $k_2 = 4.5 \times 10^8$ M^{-1} s^{-1} increases upon lowering the temperature (Figure 4), the magnitude of which corresponds to the negative activation energy $E_a = -0.3$ kcal mol^{-1}.[21]

Owing to the rapid interconversion of these Class M ion pairs (vide supra), the observed (phenomenological) rate constant k_2 is a composite of SIP and CIP contributions normalized by the ion-pair populations, that is,[7]

$$k_2 = (1 - \alpha)k_{CIP} + \alpha k_{SIP} \qquad (7)$$

Thus, the fraction of SIP from K(**C**)$^+$DNB$^-$ in THF at 20 °C is 0.14 ± 0.03,[22] which, together with the value of $k_{SIP} = 3 \times 10^9$ M^{-1} s^{-1} evaluated from K(**cryptand**)$^+$//DNB$^-$ (vide supra), leads to the SIP contribution to the electron-transfer rate of $\alpha k_{SIP} = (4.2 \pm 1.0) \times 10^8$ M^{-1} s^{-1}. Since this SIP contribution is within experimental error, the same as the observed rate constant $k_2 = (5 \pm 1) \times 10^8$ M^{-1} s^{-1} in Table 2, it is easy to calculate the CIP contribution to be minor, if at all.[22] In other words, despite the preponderant role (with $1 - \alpha \equiv 86\%$) that the contact ion pair plays in the ion-pair equilibrium, the principal pathway for the electron-transfer (self-exchange) process proceeds almost wholly via the separated ion pair K(**C**)$^+$//DNB$^-$.[23]

The same conclusion applies to the minor kinetic role played by the contact ion pair for K(**HC**)$^+$DNB$^-$ with $k_2 = 4.5 \times 10^8$ M^{-1} s^{-1}, versus the major role played by its separated ion pair, despite the minor concentration of K(**HC**)$^+$//DNB$^-$ based on $\alpha = 0.16 \pm 0.4$. Moreover, the increase in α upon lowering the temperature (see Figure 1) leads to the negative (effective) activation energy in Figure 4 and Table 1,[24] which are somewhat similar to those observed earlier.[6,7]

IV. Mechanisms of Electron-Transfer Self-Exchanges with "Separated" and "Contact" Ion Pairs of Dinitrobenzenide. The predominant presence of the dinitrobenzenide anion solely as ion-pair assemblies in THF solutions allows the SIP/CIP reactivities to be separately evaluated. As such, the quantitative evaluation of k_{SIP} and k_{CIP} in Table 2 raises two key mechanistic questions: (1) why is the value of k_{SIP} so close to the diffusion-controlled limit and (2) why is k_{SIP} almost 2 orders of magnitude faster than k_{CIP}? Before addressing these important questions, let us first consider the electron-transfer self-exchange of "free" dinitrobenzenide bereft of its counterion, since these are the predominant species extant in highly polar solvents in which the second-order rate constant is reported as $k_2 = 6 \times 10^8$ M^{-1} s^{-1}.[17] However, this fast rate process for a conceptually simple self-exchange clearly contradicts the prediction of k_2(theor) = 1×10^7 M^{-1} s^{-1} based on classical Marcus theory,[25,26] even without a correction for the vibrational component. Moreover, the inclusion of the solvent-reorganization energy would result in a barrier too high for the observed electron transfer.[27] Accordingly, we initially consider the self-exchange process to be strongly adiabatic,[28] in which case the activation barrier must include an electronic term for the donor/acceptor coupling in the transition state,[29] that is,

(21) A similar increase in the self-exchange rates at lower temperatures was also related to equilibria between the different types of aromatic ion pairs.[6,7]

(22) (a) Equation 7 is based on the fast SIP/CIP equilibration evaluated from the temperature-dependent ESR spectra in Figure S6 from which the CIP lifetime of $\tau = 10^{-9}$ s is evaluated on the basis of the rate constant for intramolecular spin exchange of 10^9 s^{-1},[10,22b] which is much faster than the characteristic time of intermolecular electron transfer of $\tau = 1/(k_2[\text{DNB}]) \approx 1 \times 10^{-8}$ s. (b) Since the strong electronic coupling between NO_2 centers obviates any sizable intrinsic barrier for electron-density redistribution within the dinitrobenzenide moiety, the intramolecular spin-exchange rate is governed by counterion switching, with ion-pair dissociation being the rate-determining step.[10]

(23) (a) The alternative evaluation of the rate data based on $k_2 = 5.3 \times 10^8$ M^{-1} s^{-1} and $\alpha = 0.14$ leads to the value of $k_{CIP} \approx 1 \times 10^8$ M^{-1} s^{-1}. (b) A relatively minor value of k_2 for the contact ion pairs derived from **C** and **HC** can be estimated as $k_2^{CIP} \leq 1 \times 10^8$ M^{-1} s^{-1}. The uncertainty derives from the difference between two larger terms (k_2 and αk_2^{SIP}), and this precludes a more accurate and meaningful analysis.

(24) (a) For K(**HC**)$^+$DNB$^-$, the calculated contribution of the separated ion pair to the overall self-exchange rate is $\alpha k_{sip} = (5 \pm 1) \times 10^8$ M^{-1} s^{-1}, which is the same (within the accuracy limit) as the observed rate constant k_2. (b) By taking into account: $k_2 \approx \alpha k_2^{SIP}$ for K(**C**)$^+$DNB$^-$ and K(**HC**)$^+$DNB$^-$, we determine the activation energy from temperature dependence of k_2 as: $E_a \approx R\Delta(\ln \alpha k_2^{SIP})/\Delta(1/T) = R\Delta(\ln k_2^{SIP})/\Delta(1/T) + R\Delta(\ln \alpha)/\Delta(1/T)$, which leads to $E_a = E_a^{sip} + \Delta H_{SEP}$.[13b] Since $E_a^{sip} = 2.5 \pm 0.5$ kcal/mol and $\Delta H_{SEP} = -2.2 \pm 0.5$ kcal/mol, the observed activation energy of intermolecular self-exchange in solutions of dinitrobenzenide with K(**C**)$^+$ or K(**HC**)$^+$ counterions is calculated to be essentially nil. Experimental values of E_a in Table 2, which agree with such a prediction (within the error margins), confirm the validity of this analysis.

(25) (a) Marcus, R. A. *Discuss. Faraday Soc.* **1960**, *29*, 21. (b) Marcus, R. A. *J. Phys. Chem.* **1963**, *67*, 853. (c) Marcus, R. A.; Sutin, N. *Biochim. Biophys. Acta* **1985**, *811*, 265. (d) Hush, N. S. *Trans. Faraday Soc.* **1961**, *57*, 557. (e) Hush, N. S. *Prog. Inorg. Chem.* **1967**, *8*, 391. (f) Hush, N. S. *Electrochim. Acta* **1968**, *13*, 1005.

(26) According to classical Marcus theory:[25] $k_2 = Z \exp(-\lambda/4RT) = 1 \times 10^7$ M^{-1} s^{-1}, where $Z = 10^{11}$ M^{-1} s^{-1} and $\lambda = 21.4$ kcal mol^{-1}.[27]

(27) (a) The reorganization energy λ for the DNB$^-$/DNB redox dyad based on the Born model for solvation has been calculated as $\lambda_o = 21.4$ kcal mol^{-1} (not including the intramolecular vibrational contribution) in DMF.[27b] (b) Eberson, L.; Shaik, S. S. *J. Am. Chem. Soc.* **1990**, *112*, 4484.

Scheme 1

$$DNB^{-} + DNB \overset{K_{IS}}{\rightleftharpoons} [DNB^{-}/DNB] \xrightarrow{k_{ET}} [DNB/DNB^{-}] \text{ etc}$$

A. Self-Exchange of Dinitrobenzenide as the "Free" Anion/"Separated" Ion Pair. In the context of the planar DNB^{-}/DNB dyad of interest here, previous investigators[29,30] have considered the incursion of the [1:1] precursor complex in the two-step electron-transfer mechanism (Scheme 1). Thus, for Scheme 1, the second-order rate constant corrected for diffusion (k_{diff}) is given as:

$$k_2 = k_{diff} k_{ET} K_{IS}/(K_{IS} k_{ET} + k_{diff}) \quad (8)$$

and

$$k_{ET} = \nu \exp(-\Delta G^*/RT) \quad (9)$$

where k_{ET} is the first-order rate constant for the inner-sphere complex and K_{IS} is its formation constant in eq 8. For the inclusion of such a precursor complex, the activation barrier (ΔG^*) must be corrected by the significant donor/acceptor electronic coupling[28,29] as well as the partial loss of solvation energy accompanying the donor/acceptor association,[31] that is,

$$\Delta G^* = (\lambda' - 2H_{DA})^2/(4\lambda') \quad (10)$$

where H_{DA} is the electronic coupling element and the modified λ' is the reorganization energy from classical Marcus theory[25] that includes the partial solvent extrusion accompanying the formation of the inner-sphere (precursor) complex.[31]

The critical precursor complex in Scheme 1 has been previously characterized structurally for various donor/acceptor dyads pertinent to analogous electron-transfer self-exchanges,[32,33] and Mairanovsky et al.[30] have presented it most recently as the face-to-face juxtaposition of the intimate DNB^{-}/DNB pair depicted as that shown in Chart 1.[34]

Experimentally, such an inner-sphere complex (IS) can usually be spectrally observed as a new absorption band in the NIR region when the acceptor (DNB) is added to the solution of the donor (DNB^{-}), but in this study, the NIR absorption appears to be partially obscured by the strongly allowed local

Chart 1

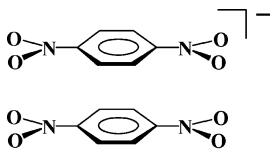

(IS)

transition of the dinitrobenzenide moiety with $\lambda_{max} = 915$ nm and $\epsilon_{max} = 22\,000\ M^{-1}\ cm^{-1}$ in THF solution (see Figure S3).[35] As a result of this ambiguity, we turn now to theoretical calculations to evaluate the activation energy for the self-exchange mechanism according to Scheme 1 in terms of (i) the electronic coupling element (H_{DA}) from the structure of precursor complex in Chart 1 and (ii) the modified reorganization energy λ' in eq 10. Thus, the coupling element (H_{DA}) is evaluated for the transition state (TS) structure obtained by adopting the face-to-face precursor structure with interplanar separation (r_{DA}) set to 3.5 Å[34] (see Chart S1 in Supporting Information) and then averaging over the precursor and successor geometries so as to yield a symmetric TS complex with overall C_i point-group symmetry. In the case of symmetry-equivalent donor and acceptor (DNB) moieties, it is convenient to evaluate H_{DA} as one-half the energy splitting of the pair of low-lying delocalized states,[36] ^2A_g and ^2A_u, that are composed primarily of symmetric and antisymmetric linear combinations of the localized (monomer) LUMOs, that is,

$$H_{DA} = {}^1/_2[E(^2A_u) - E(^2A_g)] \quad (11)$$

Various calculations at the ab initio Hartree−Fock (HF) level (restricted or unrestricted and with either 6-31G* or 6-311G* basis sets)[37] yield $H_{DA} = 2600 \pm 80\ cm^{-1}$, which is employed in the kinetic analysis reported below.[38]

For the reorganization energy, the HF calculations lead to $\lambda_{is} = 24 \pm 1.5$ kcal/mol, while inclusion of the electron correlation at the density functional theory (DFT) level (B3LYP)[37]

(28) (a) Despite the appreciable suppression of the activation barrier as a result of strong electronic coupling, the resulting adiabatic rate constant (k_2) is still slow enough so that solvent dynamics[28b] is not expected to contribute to the rate-determining step. (b) Calef, D. F.; Wolynes, P. G. *J. Phys. Chem.* **1983**, *87*, 3387.

(29) (a) Sutin, N. *Prog. Inorg. Chem*. **1983**, *30*, 441. (b) Brunschwig, B. S.; Sutin, N. *Coord. Chem. Rev.* **1999**, *187*, 233. (c) Brunschwig, B. S.; Sutin, N. In *Electron Transfer in Chemistry*; Balzani, V., Ed.; Wiley: New York, 2001; Vol. 2, p 583. (d) Compare Figure 9b in ref 10.

(30) (a) Vener, M. V.; Ioffe, N. T.; Cheprakov, A. V.; Mairanovsky, V. G. *J. Electroanal. Chem.* **1994**, *370*, 33. (b) Rauhut, G.; Clark, T. *J. Am. Chem. Soc.* **1993**, *115*, 9127. (c) Note that the strongly bound (inner-sphere) precursor complex as presented in Chart 1 (Scheme 1) merely differs *quantitatively* from the weakly bound encounter complexes previously considered in classical electron-transfer theory.[25,29] As such, we envisage a wide spectrum of noncovalently bound dyads to encompass the range of adiabatic ET rate processes.

(31) (a) For the face-to-face arrangement of the aromatic pairs, Mairanovsky et al.[30] calculated λ_o via the Kirkwood model, which relates the solvent reorganization energy for the charge redistribution accompanying electron transfer within the precursor complex (considered as a single entity surrounded by the polarizable medium). (b) We relate inner-sphere complexes in organic redox systems (of the type described herein) to the direct overlap of donor/acceptor orbitals without the intervention of solvent, in harmony with the classical description of inner-sphere complexes in inorganic systems that involve metal centers bridged by ligands in the first coordination sphere. See, for example: Taube, H. *Adv. Inorg. Chem. Radiochem.* **1959**, *1*, 1, and Fukuzumi, S.; Wong, C. L.; Kochi, J. K. *J. Am. Chem. Soc.* **1980**, *102*, 2928 and references therein.

(32) (a) Precursor complexes of planar donor/acceptor dyads have been structurally (X-ray) characterized as [1:1] complexes of tetracyanoquinodimethane with its anion radical,[32b] dichlorodicyanobenzoquinone with its anion radical,[32c] tetrathiafulvalene and its cation radical,[32d] naphthalene and its cation radical,[32e] octamethylbiphenylene and its cation radical.[32h] (b) Goldstein, P.; Seff, K.; Trueblood, K. N. *Acta Cryst*. **1968**, *B24*, 778; Hanson, A. W. *Acta Cryst*. **1968**, *B24*, 773. (c) Ganesan, V.; Rosokha, S. V.; Kochi, J. K *J. Am. Chem. Soc.* **2003**, *125*, 2559. (d) Nagayoshi, K.; Kabir, M. K.; Tobita, H.; Honda, K.; Kawahara, M.; Katada, M.; Adachi, K.; Nishikawa, H.; Ikemoto, I.; Kumagai, H.; Hosokoshi, Y.; Inoue, K.; Kitagawa, S.; Kawata, S. *J. Am. Chem. Soc.* **2003**, *125*, 221. (e) Fritz, H. P.; Gebauer, H.; Friedrich, P.; Ecker, P.; Artes, R.; Schubert, U. *Z. Naturforsch*. **1978**, *33b*, 498. (f) Le Magueres, P.; Lindeman, S.; Kochi, J. K.; *Org. Lett.* **2000**, *2*, 3567; Kochi, J. K.; Rathore, R, Le Magueres, P. *J. Org. Chem.* **2000**, *65*, 6826.

(33) For the role of such precursor complexes in the quantitative kinetics for other electron-transfer self-exchanges, see (a) Ganesan et al. in ref 32c and (b) Sun, D. L.; Rosokha, S. V.; Kochi, J. K. *J. Am. Chem. Soc.* **2004**, *126*, 1388.

(34) (a) The cofacial structure of the precursor complex is taken as a pair of juxtaposed DNB moieties separated by $r_{DA} = 3.5$ Å (Chart 1), which represents the global (average) structure of (planar) donor/acceptor dyads previously established in refs 32 b−f. Related structures with $r_{DA} = 3.3$ and 3.8 Å as well as those with "slipped" and rotated DNB moieties were also considered as discussed in the Experimental and Computational Methodologies section. (b) Despite numerous and varied attempts, we have as yet been unable to isolate crystalline $K(\mathbf{L})^+$ salts (with different ligands) of DNB/DNB^{-} associates suitable for X-ray crystallography.

(35) Note that the NIR absorption in the 1000−1200 nm range (Figure S3) could represent the low-energy tail of the precursor complex since neither DNB^{-} nor DNB alone absorb there.

(36) Newton, M. D. *Chem. Rev.* **1991**, *91*, 767.

yields an appreciably reduced value of $\lambda_{is} \approx 13.5$ kcal/mol, a result similar to those obtained in previous theoretical studies.[39] In view of the range of calculated values, we adopt an estimate of $\lambda_{is} = 19 \pm 5$ kcal/mol in the following kinetic analysis.

The solvent reorganization energy of $\lambda_{os} = 8 \pm 1$ kcal mol^{-1} is obtained from the same precursor complex (Chart 1)[30] by applying the dielectric constant of $\epsilon = 7.6$ for the THF solvent.[20] The overall reorganization energy $\lambda' = 27 \pm 5$ kcal mol^{-1} [40] together with $H_{DA} = 2600$ cm^{-1} predicts the rather low activation barrier of $\Delta G^* = 1.3$ kcal mol^{-1} in eq 10, as well as the fast rate constant of $k_{ET} = 1 \times 10^{11}$ s^{-1} in eq 9, when the pre-exponential term ($\nu = 10^{12}$ s^{-1}) is taken as previously described.[41] As a result, the observed second-order rate constant for self-exchange in Scheme 1 is calculated to lie in the range $K_{IS}k_{ET} = 5 \times 10^9$ to 5×10^{11} M^{-1} s^{-1} for this type of intermolecular π-association of planar donor/acceptor dyads that are evaluated with $K_{IS} = 0.05$ M^{-1} at one extreme and $K_{IS} = 5$ M^{-1} at the other.[42] Such fast second-order rates are indeed close to the diffusion-controlled limit, and the predicted self-exchange rate constants that lie in the range of $k_2 = 3 \times 10^9$ to 1×10^{10} M^{-1} s^{-1} are consistent with the experimentally determined value of $k_{SIP} = 3 \times 10^9$ M^{-1} s^{-1} in Table 2.[43] Since the latter pertains to electron-transfer measurements involving only the separated ion pair in eq 5, we conclude that the anionic reactivity of dinitrobenzenide is kinetically insensitive to the cationic environment that is separated by $r_{DA} \geq 6$ Å. In other words, spectral (UV−NIR, ESR) and kinetics comparisons cannot distinguish the "free" dinitrobenzenide anion in eq 4 from the "separated" ion pair in eq 5.[14e]

B. Self-Exchange of Dinitrobenzenide in "Contact" Ion Pairs. By way of contrast, the X-ray structures and spectral (UV−NIR, ESR)[9,10] as well as kinetic comparisons of the contact ion pairs: K(**L**)$^+$DNB$^-$ in Tables 1 and 2 consistently reveal the importance of the intimate binding of the ligated cations K(**BC**)$^+$, K(**C**)$^+$, and K(**HC**)$^+$ to only a single NO_2 group of the anionic dinitrobenzenide moiety. As a result, the cationic moiety can no longer be considered an innocent bystander, and at least two (principal) mechanisms must be taken into account for the participation and involvement of the counterion.

Table 3. Experimental and Theoretical Comparison of SIP and CIP Pathways in the Dinitrobenzenide Electron-Transfer Self-Exchange

	experimental		theoretical	
L	k_{SIP}[a] (M^{-1} s^{-1})	k_{CIP}[b] (M^{-1} s^{-1})	k_2(dissoc) (M^{-1} s^{-1})	k_2(assoc)[e] (M^{-1} s^{-1})
cryptand	3.0×10^9	0	$(3-10) \times 10^9$	−
C	$(4 \pm 1) \times 10^8$	$\leq 1 \times 10^8$	4×10^8 [f]	5×10^7
HC	$(5 \pm 1) \times 10^8$	$\leq 1 \times 10^8$	5×10^8 [f]	5×10^7
BC (CIP_1)	−[c]	6×10^7 [c]	−	6×10^7
BC (CIP_2)	$(5 \pm 1) \times 10^7$ [d]	$\sim 5 \times 10^7$ [d]	5×10^7 [f]	6×10^7

[a] Calculated as αk_{SIP} unless noted otherwise. [b] Calculated as $(k_2 - \alpha k_{SIP})/(1 - \alpha)$ unless noted otherwise. [c] Since CIP_1 dissociation is too slow to be involved in the intermolecular electron transfer,[47] the SIP contribution is neglected and its estimate based on $\alpha k_{SIP} = (5 \pm 1) \times 10^7$ M^{-1} s^{-1} is not valid in this case. [d] Since the rate of CIP_2 dissociation is comparable to that of intermolecular electron transfer,[43] the use of steady-state approximation (eq 7) to calculate SIP contribution as $\alpha k_{SIP} = (5 \pm 1) \times 10^7$ M^{-1} s^{-1} is questionable. [e] Calculated as $(1 - \alpha)k_{CIP}$(theor). Note that in the calculation of k_{CIP}, the values of $K_{IS} = 0.05$ and $H_{DA} = 2450$ cm^{-1} were used to equate the calculated and experimental values for the separated pathway, that is, $k_{SIP} = 3 \times 10^9$ M^{-1} s^{-1}. [f] Calculated as $\alpha(3 \times 10^9)$ M^{-1} s^{-1}.

In the *dissociative* mechanism, the critical (inner-sphere) precursor complex is attained in two steps via prior CIP separation to SIP, as shown in Scheme 2.

Scheme 2

$$\underset{\text{(CIP)}}{K(\mathbf{L})^+DNB^-} \rightleftharpoons \underset{\text{(SIP)}}{K(\mathbf{L})^+//DNB^-} \overset{DNB}{\rightleftharpoons} \underset{(IS_{SIP})}{K(\mathbf{L})^+\,[DNB^-, DNB]}$$

The *associative* mechanism, on the other hand, achieves the critical precursor complex with its counterion intact via direct CIP interaction in a single step, as shown in Scheme 3.

Scheme 3

$$\underset{\text{(CIP)}}{K(\mathbf{L})^+DNB^-} + DNB \rightleftharpoons \underset{(IS_{CIP})}{[K(\mathbf{L})^+DNB^-, DNB]}$$

Thus the essential distinction between the associative and dissociative pathways lies in the ion-pairing description of the precursor complex as either the "separated" ionic assembly (IS_{SIP}) or the "contact" ionic assembly (IS_{CIP}) prior to the electron-transfer transition state.[44]

According to the dissociative mechanism in Scheme 2, the intermolecular rate of electron transfer is controlled by the pre-equilibrium CIP/SIP separation, so that the observed rate constants is simply $k_2 = \alpha k_{SIP}$, where $k_{SIP} = 3 \times 10^9$ M^{-1} s^{-1} as expressed by eqs 8 and 9. The rate constants evaluated with the aid of the fraction α in Table 1 are listed as k_2(dissoc) in Table 3 (column 4). Analogously, the experimental measure of the intermolecular rate constant according to the associative mechanism considers the precursor complex as the "contact" ionic assembly (IS_{CIP}) in Scheme 3, so that the observed rate constant is given by $k_2 = (1 - \alpha)k_{CIP}$ where the values of k_{CIP} are evaluated from the experimental rate data according to eq 7 and listed as k_2(assoc) in Table 3 (column 5).

(37) Pople, J. A. et al. *Gaussian 98*, revision A.11.3; Gaussian, Inc.: Pittsburgh, PA, 2001.
(38) Additional calculations based on DFT yielded a smaller estimate of ~1600 cm^{-1}. Further details of the H_{DA} calculation are given in the Experimental and Computational Methodologies section.
(39) (a) Klimkans, A.; Larsson, S. *Chem. Phys.* **1994**, *189*, 25. (b) Blomgren, F.; Larsson, S.; Nelsen, S. F. *J. Comput. Chem.* **2001**, *22*, 655.
(40) (a) Note that $\lambda' = 27$ kcal mol^{-1} predicts the intervalence absorption band at $\lambda_{IV} = 1050 \pm 150$ nm (or roughly 9000 cm^{-1}) that is easily within the experimental limits of our tentative spectral assignment.[35] Most importantly, the value of $H_{DA} < \lambda'/2$ assigns the precursor complex to a class II mixed-valence anion,[40c] according to the Robin−Day formalism.[36b] See: (b) Robin, M. B.; Day, P. *Adv. Inorg. Chem. Radiochem.* **1967**, *10*, 247. (c) Also see Brunschwig and Sutin in ref 29.
(41) Since such electron-transfer self-exchanges involve numerous molecular (~500−3000 cm^{-1}) and solvent (~10−100 cm^{-1}) vibrational modes, the pre-exponential factor $\nu = (\Sigma\nu_i^2\lambda_i/\Sigma\lambda_i)^{1/2}$ is difficult to rigorously calculate from the available data. Thus we have taken $\nu = 10^{12}$ s^{-1}, which is the same value as previously used for the description of electron transfer in the intermolecular anion-radical self-exchanges.[32c]
(42) (a) Such limits were chosen because the formation constants of most anion-radical complexes with their parent acceptor[32c] as well as those of more conventional charge-transfer complexes[42b,c] lie in the 0.05−5 M^{-1} range. See, for example: (b) Foster, R. *Organic Charge-Transfer Complexes*; Academic: New York, 1969. (c) Mulliken, R. S.; Person, W. B. *Molecular Complexes*; Wiley: New York, 1969. (d) Andrews, L. J.; Keefer, R. M. *Molecular Complexes in Organic Chemistry*; Holden-Day: San Francisco, CA, 1964.
(43) If we consider such a kinetic equivalence between free DNB$^-$ and its separated ion pair, we evaluate the pre-equilibrium constant as $K_{IS} = 0.05$ M^{-1} from the experimentally determined value of $k_{SIP} = 3 \times 10^9$ M^{-1} s^{-1}.
(44) (a) Associative and dissociative mechanisms correspond to earlier Marcus classifications.[4a] (b) Note that the inner-sphere precursor complex is the intermolecular analogue to the intramolecular electron transfer for the bridged systems considered by Marcus.[4a] For equivalency of such an intermolecular precursor complex with electron transfer in bridged mixed-valence systems, see: (c) Sun, D. L.; Rosokha, S. V.; Lindeman, S. V.; Kochi, J. K. *J. Am. Chem. Soc.* **2003**, *125*, 15950 and Sun et al. in ref 33.

Scheme 4

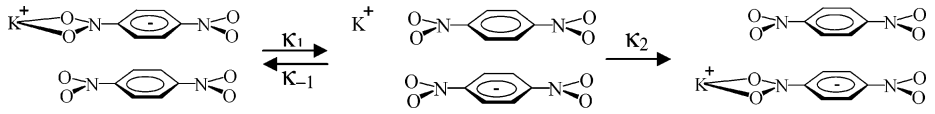

Comparisons of the values of k_2(dissoc) and k_2(assoc) in Table 3 with the observed second-order rate constant (k_2) in Table 2 indicate that the relevant ion-pair pathway for intermolecular electron transfer is notably dependent on the ligation of the potassium cation, that is, K(**L**)$^+$. For the ligand **L** = **cryptand**, ionic dissociation is clearly irrelevant, and the electron-transfer pathway proceeds solely via the inner-sphere (precursor) complex in Chart 1. Likewise for **L** = 18-crown-6 (**C**) and the dicyclohexano analogue (**HC**), the principal pathway for the electron-transfer involves prior ion-pair separation to the separated ion pairs K(**C**)$^+$//DNB$^-$ and K(**HC**)$^+$//DNB$^-$, respectively. However, the same rate comparison attendant upon K$^+$ ligation by dibenzo-18-crown-6 in K(**BC**)$^+$DNB$^-$ favors the associative pathways for both CIP_1 and CIP_2. This conclusion is strongly reinforced for CIP_1 by independent ESR measurements for the *rate* of CIP/SIP interconversion of $k_{SEP} < 10^6$ s^{-1}, which is clearly too slow to accommodate the observed electron-transfer rate of $k_2 = 6 \times 10^7$ M^{-1} s^{-1}.[45] For CIP_2, the separation rate (estimated to be $k_{SEP} \approx 10^7$ s^{-1}) is comparable to the rate of intermolecular electron transfer,[46] and associative and dissociative pathways are likely to be competitive.[47]

Let us now briefly consider why the rate of intermolecular (self-exchange) electron transfer for the contact ion pair is roughly 2 orders of magnitude slower than that of the separated ion pair. Although the theoretical formulation of electron transfer within the precursor complex (IS_{SIP}) in Scheme 2 is well accommodated by eqs 9 and 10, that for the associative pathway must recognize the attendant movement of the counterion within IS_{CIP}, which for clarity is pictorially presented as:

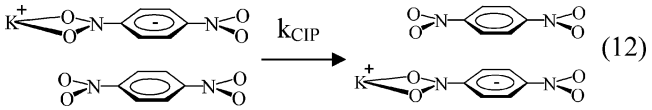

(12)

To deal with this theoretical complexity, Marcus[4a] dissected the problem into two discrete processes (Scheme 4), in which the first step is conceptually akin to the intramolecular electron transfer in a (unsymmetrical) mixed-valence complex,[29c] and the second step represents cationic migration under similar circumstances. As such, the kinetics formulation for the overall (CIP) process in Scheme 4 is:

$$k_{ET}' = \kappa_1\kappa_2/(\kappa_{-1} + \kappa_2) \qquad (13)$$

Following the traditional approach to the solution of these (standard) problems,[4a] we calculate $\kappa_1 = 1.6 \times 10^{10}$ s^{-1}, $\kappa_{-1} = 5 \times 10^{11}$ s^{-1}, and $\kappa_2 = 5 \times 10^{10}$ s^{-1} as described in the Experimental and Computational Methodologies section, and these values lead to $k_{ET}' = 1.5 \times 10^9$ s^{-1} according to eq 13. The inclusion of the pre-equilibrium constant for the formation of inner-sphere complex as $K_{IS} = 5 \times 10^{-2}$ M^{-1} leads to the calculated value of intermolecular rate constant for the contact ion pair as $k_{CIP}^{theor} = 7 \times 10^7$ M^{-1} s^{-1}, which is rather close to the experimental value of $k_2 = 6 \times 10^7$ M^{-1} s^{-1} in Table 3.

Finally, on the basis of the relative magnitudes of the rate constants in eq 13, we judge that the cationic migration component of Scheme 4 contributes roughly half the electron-transfer component to the overall kinetics. Such a conclusion underscores the need to explicitly consider ionic mobility for moderating redox reactivities in the design of new contact ion pairs, which we hope will be the subject of further studies.

Summary and Conclusion

The three distinctive ion pairs composed of Classes S, C, and M allow the complex ion-pair kinetics of K(**L**)$^+$DNB$^-$ salts in THF solutions to be unambiguously dissected by the combination of X-ray crystallography and spectral (UV−NIR, ESR) analyses. For intermolecular electron transfer between the *p*-dinitrobenzene acceptor (DNB) and its radical anion (DNB$^-$), the observed second-order rate constant (k_2) is essentially the same as that (k_{SIP}) in the separated ion pair with K(**cryptand**)$^+$// DNB$^-$. Thus, for the second-order processes with either the "free" nitrobenzenide anion or the "separated" ion pair, $k_2 \approx k_{SIP} = 3 \times 10^9$ M^{-1} s^{-1}, which is close to the diffusion-controlled limit and too fast to be accommodated by classical Marcus theory. However, the inclusion of the discrete [1:1] intermediate [DNB$^-$/DNB] as the critical precursor complex in the two-step mechanism for self-exchange (Scheme 1) leads to the correct prediction of the observed rate constant (k_2) when it is included in the two-state Marcus−Sutin formulation by the theoretical computation of the electronic coupling element (H_{DA}) and reorganization energy (λ') from the inner-sphere complex according to Chart 1.

To accommodate the significantly slower self-exchange rates with the contact ion pair, $k_{CIP} = 6 \times 10^7$ M^{-1} s^{-1}, the two-state calculation of the precursor complex invokes the direct (associative) mechanism in Scheme 3. As such, the formation of the precursor complex (IS_{CIP}) can be conveniently dissected into two discrete steps in which the electron-transfer component is separately evaluated from the cationic migration within the inner-sphere complex (Scheme 4).

Dinitrobenzenide as a mixed-valence anion thus offers a unique opportunity to examine quantitatively the roles of both

(45) The lifetime of CIP_1: $\tau > 10^{-6}$ s is evaluated from the rate constant of intramolecular spin exchange ($< 10^6$ s^{-1}),[10,22b] which is much longer than the characteristic time for intermolecular electron transfer, that is, $\tau = 1/(k_2[DNB]) \approx 1 \times 10^{-7}$ s.

(46) The CIP_2 lifetime of $\tau \approx 10^{-7}$ s is evaluated from the rate constant for intramolecular spin exchange ($\approx 10^7$ s^{-1}),[10,22b] which is comparable to the characteristic time of intermolecular electron transfer, that is, $\tau = 1/(k_2[DNB]) \approx 1 \times 10^{-7}$ s.

(47) The slightly different kinetic behavior of CIP_1 and CIP_2 follows from their distinctive interionic bindings, that is:

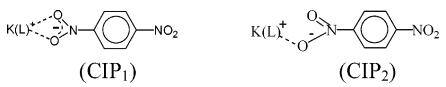

(CIP_1) (CIP_2)

previously described as bidentate and monodentate, respectively.[10]

"separated" and "contact" ion pairs in donor and acceptor reactivities. Whereas the redox properties of free anions and their separated ion pairs are not expected to differ significantly if the interionic separation exceeds ~6 Å, a more complex picture emerges for the reactivity of contact ion pairs. Therefore, we believe that ionic ligation of the type described here for K(**L**)$^+$ offers a promising approach to further examine how the ligand actually tunes ionic reactivity.

Experimental and Computational Methodologies

Solvents, neutral *p*-dinitrobenzene, and its anion-radical salts (with potassium ligated with macrocyclic polyethers) were prepared and handled as described earlier.[9,10] Electronic spectra were measured on either a Hewlett-Packard 8453 diode array or a Varian Cary 5 spectrometer, ESR measurements were performed on a Bruker ESP-300 X-band spectrometer, and structural studies were carried out with a Bruker SMART APEX diffractometer.[9,10] The hyperfine splitting constants were determined via computer simulation of the ESR spectra of pure anion-radical salts using Bruker WINEPR Simfonia program. The equilibrium constants between different forms of ion pairs of dinitrobenzenide were determined by simulation of the electronic and ESR spectra as the superposition of CIP and SIP components (with double integration of each ESR constituent), as described previously.[10] Thermodynamic parameters for CIP isomerization (eq 2) were determined from the linear temperature dependence of ln K_{ISOM} with T^{-1} (see Figure S2 in Supporting Information). Thermodynamic parameters for the CIP/SIP equilibria according to eq 1 (eq 3) were determined from the dependence of T^{-1} with ln K_{SEP}, where K_{SEP} = [SIP]/[CIP] as shown in the inset of Figure 1.[13]

ESR Study of Self-Exchange. Kinetic parameters for intermolecular (DNB^{-}/DNB) electron transfer were determined from the (general) ESR line broadening of *p*-dinitrobenzene anion radical in the presence of added (neutral) acceptor as follows.

(a) For K(**cryptand**)$^+DNB^-$, the ESR line width ($\Delta H \approx 0.3$ G) of the THF solution of the pure salt was essentially independent of concentration (within the practicable concentration range 0.5−2 mM). Addition of 3−5 mM of neutral acceptor resulted in the significant broadening of all the lines (Figure 3), and line widths were measured at various concentrations of the neutral acceptor by computer simulation (Simfonia program) in the slow-exchange limit (i.e., with individual lines). Line width increase relative to that of solution of the pure anion radical ($\Delta\Delta H$) was proportional (at constant temperature) to the concentration of the added neutral DNB, indicating that broadening was related to the electron-transfer self-exchange process.[17,18] Line width measurements at various concentrations of DNB (at constant temperature) led to the second-order rate constant as[17,18] $k_2 = 1.52 \times 10^7 \Delta\Delta H/(1 - P_j)$[DNB], where $\Delta\Delta H$ is the increment in peak-to-peak line width (in gauss) due to the electron self-exchange, [DNB] is the concentration (in mol/L) of the parent acceptor, and the correction $(1 - P_j)$ takes into account the hyperfine line used (with $P_j = 0.2$ for the ESR spectrum of K(**cryptand**)$^+DNB^-$). Such measurements were performed at several temperatures, and the dependence of ln k_2 on $1/T$ afforded the activation energies listed as E_a.

(b) For K(**BC**)$^+DNB^{\bullet-}$, the ESR spectrum of THF solutions of the pure salt was successfully represented as the superposition of ESR spectra of three components: viz. a pair of "localized" species, CIP_1 and CIP_2, and the small (~1−2%) fraction of SIP (Figure 2). Addition of neutral DNB resulted in the broadening of the ESR spectrum (Figure 5), which could be simulated (see Figure S4) as broadened CIP_1 and CIP_2 components and a single line corresponding to the SIP fraction (vide infra). The ESR line widths for CIP_1 and CIP_2 were measured in the presence of various DNB concentrations in slow exchange limit leading (as described above for K^+(**cryptrand**)DNB^- salt) to the rate constant k_2, and temperature dependence of k_2 afforded the activation energies E_a. Measurable broadening of CIP_1 and CIP_2 lines was observed at high (~100 mM) concentrations of DNB. Under these conditions, the SIP component of the ESR spectrum coalesces into one line, indicating that the self-exchange of SIP reached the fast-exchange limit (Figure S4). Note that, in the presence of DNB, the SIP fraction in THF solution of the pure K($\mathbf{L}_{E3}$)$^+DNB^{\bullet-}$ salt increased by roughly 3−5%, which was attributed to the additional channel for ion-pair dissociation associated with intermolecular electron transfer.

(c) For K(**C**)$^+$ $DNB^{\bullet-}$ and K(**HC**)$^+DNB^{\bullet-}$, the THF solutions of anion radicals were characterized by nearly identical ESR spectra, with hyperfine-splitting patterns assigned to fast intramolecular spin exchange between their nonequivalent NO_2 groups.[10] Addition of ~10 mM dinitrobenzene led to the broadening of spectra (Figure S5), and at [DNB] ~50 mM, the lines coalesce into a single broad line. Since the alternating line broadening (Figure S6) complicated the ESR spectral behavior of K(**C**)$^+DNB^{\bullet-}$ and K(**HC**)$^+DNB^{\bullet-}$ in the slow exchange limit (where individual lines were observed), the kinetics of their intermolecular ET processes were studied in the fast-exchange limit at concentrations of neutral DNB of approximately 100−300 mM. (Note that the kinetics correspondence at the fast and slow exchange limits was established earlier for other anion-radical systems.[17]) Under such conditions, the increase in the concentration of neutral DNB was accompanied by the narrowing of the single (broad) line. Line widths measured at constant temperature led to the self-exchange rate constant as[17] $k_2 = 2.05 \times 10^7 \nabla/\Delta H$[c], where ΔH is the corrected line width (G), which was obtained by subtracting the intrinsic line width in the absence of exchange from the line width in the presence of exchange, and ∇ is the second moment of the unbroadened spectrum (G^2). The temperature dependence of k_2 afforded the activation barriers listed in Table 2.

Theoretical Evaluation of the Electronic Coupling in the Inner-Sphere Complex of Dinitrobenzene. The structure of the precursor complex was based on the structures of isolated complexes of other anion and cation radicals with their neutral precursors, as well as the structures of conventional charge-transfer complexes.[32,42] The characteristic feature of such associates is the parallel arrangement of two planar moieties that lie cofacially atop one another (and possibly somewhat shifted laterally) with an interplanar separation (r_{DA}) of about 3.3−3.5 Å. The structures of the neutral and anion-radical components of the precursor (and successor) complexes were based on the X-ray crystal data for the neutral DNB and the separated ion pair, K(**cryptand**)$^+$//DNB^-, respectively.[10] These structures were then slightly modified to yield precise C_i point-group symmetry for each monomer (i.e., inversion symmetry). The transition-state structure (TS, denoted as structure A in Chart S1, Supporting Information) was then obtained by averaging over the precursor and successor structures, so as to yield a TS with overall C_i symmetry (approximate D_{2h} symmetry) and adopting a mean value of $r_{DA} = 3.5$ Å. Application of the two-state electronic model[36] is expected to be reasonable for such direct (through-space) coupling between the cofacial (donor/acceptor) dyads in Chart 1. Additional precursor structures were generated to assess the sensitivity of H_{DA} to intermolecular displacements. The electron-exchange process involved the LUMO of the neutral DNB and the corresponding SOMO (singly occupied MO) of dinitrobenzene radical anion. These orbitals have A_u symmetry in the local C_i point group of each monomer (a schematic depiction of the monomer LUMO(SOMO) is given in Chart S1). Since all contributions to the LUMO(SOMO) from atoms along the NN axis have the same phase, good overlap was expected for this juxtaposed (cofacial) TS geometry, and it was also likely to be maintained for lateral displacement of the monomers in

(48) (a) Braga, P. *Chem. Phys. Lett.* **1991**, *213*, 159. (b) Braga, M.; Larsson, S. *Chem. Phys. Lett.* **1991**, *213*, 217. (c) Curtiss, L. A.; Naleway, C. A.; Miller, J. R. *Chem. Phys.* **1993**, *176*, 387. (d) Curtiss, L. A.; Naleway, C. A.; Miller, J. R. *J. Phys. Chem.* **1993**, *97*, 4050. (e) Kim, K.; Jordan, K. D.; Paddon-Row, M. N. *J. Phys. Chem.* **1994**, *98*, 11053.

(49) (a) Cai, Z.-L.; Sendt, K.; Reimers, J. R. *J. Chem. Phys.* **2002**, *117*, 5543. (b) Dreuw, A.; Head-Gordon, M. *J. Am. Chem. Soc.* **2004**, *126*, 4007. (c) Tozer, D. J. *J. Chem. Phys.* **2003**, *119*, 12697. (d) Lappe, J.; Cave, R. J.; Newton, M. D.; Rostov, I. V. *J. Phys. Chem.* **2005**, *109*, 6610.

the direction of the NN axes (e.g., structure B, with the relative displacement of 4.2 Å). On the other hand, the monomer displacement in the direction perpendicular to the NN (and interplanar) axis was expected to yield some destructive interference (and hence, somewhat poorer overlap) due to the nodal structure of the orbitals (see Chart S1). As an example, we generated structure C, based on lateral displacements of 2.1 and 1.2 Å, respectively, along the NN axis and perpendicular to it. Finally, we have generated two variants of structure A by assigning $r_{DA} = 3.3$ Å (structure D) and $r_{DA} = 3.8$ Å (structure E) summarized in Chart S1. For such complexes, the following values of H_{DA} (in cm^{-1}) were obtained: 2600 (A), 1676 (B), 1213 (C), 3350 (D), and 1616 (E). Note that the variation of H_{DA} in structures A, D, and E (with r_{DA} varying from 3.3 to 3.8 A) gave a value of β (3.1 $Å^{-1}$), which is quite reasonable for through-space coupling, where β is the mean exponential decay coefficient of $|H_{DA}|^2$ with r_{DA}.[36]

The coupling term H_{DA} has often been viewed as an effective one-electron matrix (or resonance) element, which when expressed as an energy gap (according to eq 11) involves the cancellation of the electron-correlation terms that contribute to the individual state energies.[36] Nevertheless, the influence of the electron correlation on the magnitude of H_{DA} has been considered in the literature,[39b,48] using post-Hartree−Fock or DFT methods. For bridge-mediated coupling, electron-correlation effects have been frequently found to be modest, although cases of systematic reduction in the magnitude of H_{DA} have been observed (see, for example, Larsson et al. in ref 39b). In the present case of direct (through-space) coupling, DFT calculations based on the B3LYP functional[37] yielded an energy splitting (and hence H_{DA} magnitude) that was roughly 60% of the HF value.[38] An artifactual tendency to underestimate charge-transfer energy gaps by DFT methods has been noted,[49] and thus the present DFT results were considered to give a lower limit for the gap.

Theoretical Evaluation of λ_{is}. Using isolated neutral (n) and radical-anion (a) monomers, we evaluated λ_{is} at both the HF and DFT levels. Defining the total monomer energy as $E_i(\mathbf{r})$, where i = n or a, and $\mathbf{r}$ is the set of internal molecular coordinates, we can express the vibrational component λ_{is} of the reorganization energy as the following sum of values for the neutral and anionic monomers, respectively:[39b,50]

$$\lambda_{is} = \lambda_{is}(n) + \lambda_{is}(a) \tag{14}$$

where

$$\lambda_{is}(n) = E_n(\mathbf{r}_a) - E_n(\mathbf{r}_n) \tag{15}$$

$$\lambda_{is}(a) = E_a(\mathbf{r}_n) - E_a(\mathbf{r}_a) \tag{16}$$

and $\mathbf{r}_n$ and $\mathbf{r}_a$ are the optimized coordinates of the neutral and anion monomer, respectively. For perfect harmonic behavior, where neutral and anion species have the same force constants, we would have:

$$\lambda_{is}(n) = \lambda_{is}(a) \tag{17}$$

The HF calculations (with 6-31G* and 6-311G* basis sets, and either restricted or unrestricted open shell anions)[37] yielded $\lambda_{is} = 24 \pm 1.5$ kcal/mol. The unrestricted DFT level (using the same 6-31G* basis and the B3LYP functional)[37] yielded a smaller estimate: $\lambda_{is} = 13.5$ kcal/mol. In all cases, $\lambda_{is}(n)$ and $\lambda_{is}(a)$ were the same to within 3%.

On the basis of the calculated values of the electronic coupling element (H_{DA} in the range from 1600 to 3200 cm^{-1}, vide supra) and with $\lambda = 27$ kcal mol^{-1}, the barrier for electron transfer was calculated from eq 10 to lie in the range from 0.6 to 2.9 kcal mol^{-1}. Low barriers resulted in high electron-transfer rate constants (calculated via eq 9) in the range from 8×10^9 to 6×10^{11} s^{-1}. Such a fast first-order electron transfer led (via eq 8) to second-order rate constants in agreement with experiment. Thus, despite possible structural variations of the precursor complex, the strong electronic coupling assured low barriers and high rates of electron transfer (for reasonable geometries).

Calculation of the Electron-Transfer Rate Constants for Contact Ion Pairs. According to Marcus,[4a] the overall electron transfer for a precursor complex involving a contact ion pair in eq 12 (i.e., for the systems in which electron transfer precedes counterion migration) is presented in Scheme 4, with rate constant k_{ET}' expressed in terms of the rate constant for unsymmetrical electron transfer (endergonic for κ_1 and exergonic for κ_{-1}) and the rate constant for cation migration κ_2 in eq 13. The calculation of the rate constants κ_1 and κ_{-1} for unsymmetrical electron transfer was based on eq 9, with the barrier ΔG^* calculated according Sutin et al. as:[29] $\Delta G^* = \lambda/4 + \Delta G°/2 + (\Delta G°)^2/4/(\lambda - 2H_{DA}) - H_{DA} + H_{DA}^2/(\lambda + \Delta G°) - H_{DA}^4\Delta G°/(\lambda + \Delta G°)^4$. In this expression, the values of $\lambda = 27$ kcal mol^{-1} and $H_{DA} = 2600$ cm^{-1} were taken to be the same as those used in the calculation of electron transfer with the separated dinitrobenzenide. Free-energy changes for electron transfer $\Delta G° = 2.1$ and -2.1 kcal mol^{-1} for the forward and back electron transfer, respectively, within the IS_{CIP} were calculated as the electrostatic interaction of potassium cation with the electron residing on the coordinated and uncoordinated dinitrobenzene within the IS_{CIP} as: $\Delta G° = (1/r_1 - 1/r_2) \times e^2/\epsilon$ with $r_1 = 5.0$ Å, $r_2 = 6.9$ Å, and $\epsilon = 7.5$. These led to the values of the activation barriers for the forward and back electron transfer as $\Delta G^‡ = 2.5$ and 0.4 kcal mol^{-1}, respectively, and to the rate constants $\kappa_1 = 1.6 \times 10^{10}$ and $\kappa_{-1} = 5 \times 10^{11}$ s^{-1}. The rate constant for cation migration was calculated according to Marcus[4a] as $\kappa_2 = k_{diff}\pi/(16a^2R) = 5 \times 10^{10}$ s^{-1}, where $k_{diff} = 1.27 \times 10^{10}$ M^{-1} s^{-1} is the diffusion rate constant, $R = 5$ Å is the reaction radius, and $a = 3.5$ Å is the distance for potassium migration within the precursor complex. On the basis of the values of κ_1, κ_{-1}, and κ_2, the overall (first-order) electron-transfer rate constant within IS_{CIP} was calculated from eq 13. The value of k_{ET}' together with k_{diff} and K_{IS} (which was taken to be the same as that for the separated ion pair) allowed the calculation of the second-order (self-exchange) rate constant according to eq 8.

Acknowledgment. S.V.R., J.-M.L., and J.K.K. thank the R. A. Welch Foundation and National Science Foundation for financial support, and M.D.N. was supported by the Division of Chemical Sciences, U.S. Department of Energy, under Grant DE-AC02-98CH10886.

Supporting Information Available: UV−NIR spectra (in THF and solid-state) of Class S, M, and C ion-pair salts (Figure S1); thermodynamics of the CIP_1/CIP_2 isomerization for K(**BC**)$^+$DNB$^-$ in THF (Figure S2); NIR spectrum of K(**cryptand**)$^+$DNB$^-$ in the presence of neutral DNB (Figure S3); simulation of ESR spectrum of K(**BC**)$^+$DNB$^-$ (measured in the presence of neutral DNB) as superposition of broadened spectra of CIP_1, CIP_2, and SIP (Figure S4); ESR line broadening upon addition of DNB to THF solution of K(**C**)$^+$DNB$^-$ (Figure S5); dynamic ESR simulation of alternating line broadening for K(**C**)$^+$DNB$^-$ (Figure S6); simulation of ESR spectrum of K(**HC**)$^+$DNB$^-$ as superposition of CIP and SIP (Figure S7); shape of LUMO of DNB and hypothetical structures of precursor complex (Chart S1); and complete ref 37. This material is available free of charge via the Internet at http://pubs.acs.org.

JA051063Q

(50) Perng, B.-C.; Newton, M. D.; Raineri, F. O.; Friedman, H. L. *J. Chem. Phys.* **1996**, *104*, 7153.